PHYSICAL REVIEW A **66**, 013808 (2002)

Class-*A* lasers with injected signal: Bifurcation set and Lyapunov–potential function

Catalina Mayol,[1,2] Raúl Toral,[1,2] Claudio R. Mirasso,[1] and Mario A. Natiello[3]
[1]*Departament de Física, Universitat de les Illes Balears, E-07071 Palma de Mallorca, Spain*
[2]*Instituto Mediterráneo de Estudios Avanzados (IMEDEA, CSIC-UIB), Campus UIB, E-07071 Palma de Mallorca, Spain*
[3]*Centre for Mathematical Sciences, Lund University, S-22100 Lund, Sweden*
(Received 14 January 2002; published 17 July 2002)

We describe the bifurcation set for a class-*A* laser with an external injected signal in terms of the amplitude and the frequency of the applied field. We explain the dynamical behavior of this kind of lasers in terms of a Lyapunov potential in the case where such a description is possible. In particular, a full description for the deterministic and nondeterministic dynamics can be given by using the Lyapunov potential for some of the external parameters. Depending also on the value of these parameters, the phase of the electric field drifts with time in the stochastic case.

DOI: 10.1103/PhysRevA.66.013808 PACS number(s): 42.65.Sf, 42.55.Ah, 42.60.Mi

I. INTRODUCTION

To control a laser using an injected signal is an active area of research with a great variety of applications. Experiments show that a very rich behavior (locking, pulses, multistability, etc.) can appear depending on the range of parameters considered [1–4]. This paper studies the dynamics of a class-*A* lasers in the presence of an external electric field. By means of analytical and numerical studies, we obtain the complete deterministic bifurcation set for this system. As a main result, we determine the locking range, i.e., the range of parameters for which the frequency of the emitted light equals that of the injected signal, as well as the different regions of multistability. In the case that the stochastic terms corresponding to the spontaneous emission are considered, we predict the existence of a noise-induced shift of the laser frequency.

Our starting point will be a simple description of laser dynamics in terms of rate equations for the temporal evolution of the different system variables. It is usual to classify lasers according to the decay rate of photons, carriers, and material polarization [1,5,6]. In the so-called class-*A* lasers the material variables decay to the steady state much faster than the electric field, and can therefore be adiabatically eliminated. The resulting equation for the electric field suffices to describe the dynamical evolution of the laser. This equation contains a white-noise term accounting for the stochastic nature of the spontaneous emission. Some properties of typical class-*A* lasers, such as a dye laser, are discussed in Refs. [7,8].

In a previous paper [9] we have analyzed the dynamics of class-*A* lasers, in the absence of an external forcing, by using a Lyapunov-potential function [10]. The deterministic dynamics (neglecting the spontaneous emission noise) has been completely understood as a movement of a fictitious test particle on the surface of the Lyapunov potential. In the presence of spontaneous emission noise, the probability density function obtained from the potential makes possible the calculation of stationary averages of interest [11,12], such as the above-mentioned noise-induced frequency shift of the emitted light.

It is the aim of this paper to study class-*A* lasers with an injected field in order to determine the bifurcation set and to describe the deterministic dynamics, whenever possible, in terms of a Lyapunov potential. In the stochastic case, the same Lyapunov potential will allow us to calculate mean values in the steady-state limit. We will consider both the cases where the detuning frequency between the injected signal and the unperturbed laser is equal to zero and different from zero.

The paper is organized as follows. In Sec. II, we present the model equations for a class-*A* laser with injected signal used in the remaining sections. In Sec. III, we determine the bifurcation set in terms of the amplitude and frequency of the injected signal. In Sec. IV, we describe the laser dynamics in terms of a potential function, valid for the case of a zero-detuning injected signal, and discuss its relevance both in the deterministic and stochastic dynamics. Finally, we summarize the main results in Sec. V.

II. EQUATIONS

We consider a class-*A* laser [5] whose dynamics can be described in terms of the slowly varying complex amplitude E of the electric field. The physical electric field is given by $\mathcal{E}(t)=e^{i\Omega_0 t}E(t)+\text{c.c.}$ To this system we inject a monochromatic optical field $Se^{i\Omega t}$ of amplitude S and frequency Ω. The resulting evolution equation is [13,14]

$$\dot{E}(t)=(1+i\alpha)\left(\frac{\Gamma}{1+\beta|E|^2}-\kappa\right)E+\sigma S e^{-i\Delta\Omega t}+\zeta(t), \tag{1}$$

where $\Delta\Omega=\Omega_0-\Omega$ is the detuning between the external field and the unperturbed laser operating frequency Ω_0. κ, Γ, β, α, and σ are (real) intrinsic laser parameters: κ is the cavity decay rate, Γ the gain parameter, β the saturation-intensity parameter, α the *atomic detuning* parameter, and σ the amplitude feed-in rate, proportional to the inverse of the round–trip time τ_{in} [15]. Another widely used model expands the nonlinear gain term, proportional to β, to give a cubic dependence on the field (third-order Lamb theory [16]). $\zeta(t)$ is a complex Langevin source term accounting for

the stochastic nature of spontaneous emission. It is taken as a Gaussian white noise of zero mean and correlations

$$\langle \zeta(t)\zeta^*(t')\rangle = 4D\,\delta(t-t'), \tag{2}$$

where D measures the strength of the noise.

In the nonforcing situation, $S=0$, the deterministic version, $D=0$, of Eq. (1) has two fixed points. The fixed point $E=0$, the *off* solution, corresponds to a situation in which the laser is not emitting light. This solution is unstable for $\Gamma>\kappa$ when the laser switches to the *on* solution (or *lasing mode* of operation) with a nonzero light intensity given by $|E|^2=(\Gamma-\kappa)/(\kappa\beta)$.

By writing $E=(x_1+ix_2)e^{-i\Delta\Omega t}$, i.e., (x_1,x_2) are the real and imaginary parts of the electric field E in the reference system that rotates with frequency $-\Delta\Omega$, and introducing a new dimensionless time such that $t\to\kappa t$, the evolution equations become

$$\dot{x}_1=\left(\frac{a}{b+x_1^2+x_2^2}-1\right)(x_1-\alpha x_2)+\rho-\omega x_2+\xi_1(t)\cos(\omega t) - \xi_2(t)\sin(\omega t), \tag{3}$$

$$\dot{x}_2=\left(\frac{a}{b+x_1^2+x_2^2}-1\right)(\alpha x_1+x_2)+\omega x_1+\xi_1(t)\sin(\omega t) + \xi_2(t)\cos(\omega t), \tag{4}$$

where $a=\Gamma/(\kappa\beta)$, $b=1/\beta$, $\rho=\sigma S/\kappa$, $\omega=\Delta\Omega/\kappa$, and $\zeta(t)=\xi_1(t)+i\xi_2(t)$ introduces real white-noise processes with zero mean and correlations,

$$\langle \xi_i(t)\xi_j(t')\rangle = 2\epsilon\delta_{ij}\delta(t-t'), \tag{5}$$

with $\epsilon=D/\kappa$. The statistical properties that follow from the set of equations (3)–(4) are contained in the Fokker-Planck equation for the time evolution of the probability density function [17]. A simpler, yet equivalent set of equations, in the sense that they give rise to the same Fokker-Planck equation, is [8]:

$$\dot{x}_1=\left(\frac{a}{b+x_1^2+x_2^2}-1\right)(x_1-\alpha x_2)+\rho-\omega x_2+\xi_1(t), \tag{6}$$

$$\dot{x}_2=\left(\frac{a}{b+x_1^2+x_2^2}-1\right)(\alpha x_1+x_2)+\omega x_1+\xi_2(t). \tag{7}$$

These equations can be written in terms of the intensity I and phase ϕ, by making the change of variables $x_1=\sqrt{I}\cos(\phi)$ and $x_2=\sqrt{I}\sin(\phi)$,

$$\dot{I}=2\left[\frac{a}{b+I}-1\right]I+2\rho\sqrt{I}\cos(\phi)+2\sqrt{I}\xi_I(t), \tag{8}$$

$$\dot{\phi}=\alpha\left[\frac{a}{b+I}-1\right]-\frac{\rho}{\sqrt{I}}\sin(\phi)+\omega+\frac{1}{\sqrt{I}}\xi_\phi(t), \tag{9}$$

where $\xi_I(t)$ and $\xi_\phi(t)$ are white-noise processes of mean zero and correlations (5). The multiplicative terms of these equations have to be understood in the Stratonovich sense [17]. We remind the reader that, in this interpretation, an integral of the form, e.g., $\int_t^{t+h}F(I(s))\xi_I(s)ds$ has to be understood, in the limit of $h\to 0$, as $\frac{1}{2}[F(I(t))+F(I(t+h))]\int_t^{t+h}\xi_I(s)ds$, for any arbitrary function $F(I)$.

In the next sections, the system of equations (6),(7) is studied. For convenience, we will switch between the descriptions (6),(7) and (8),(9) whenever it simplifies the discussion.

III. BIFURCATION SET

We consider throughout this section the deterministic version of Eqs. (6),(7) or (8),(9) obtained by neglecting all the stochastic terms or, equivalently, by setting $\epsilon=0$. It is easy to observe that any trajectory remains bounded in the (x_1,x_2) plane. This comes from the asymptotic form of Eq. (8) in the limit $I\to\infty$, namely, $\dot{I}=-2I$, which shows that trajectories with a large intensity I are restored towards the origin. Consequently, the only asymptotic behavior of Eqs. (6),(7) can be a fixed point or a periodic orbit. Remember that Eqs. (6),(7) are written in the reference frame that rotates with frequency $-\omega$. Therefore, a fixed point solution represents a situation in which the frequency of the laser electric field E equals that of the injected electric field. We are interested in finding the *locking range*, i.e., the set of parameters (ρ,ω) for the injected field, such that there exist *stable* fixed point solutions, also called *locking* solutions.

A. The fixed point solutions

The intensity I_s and phase ϕ_s of the fixed points are found by setting $\dot{I}=\dot{\phi}=0$ in Eqs. (8) and (9). The resulting equations can be rewritten as

$$\rho^2=I_s\left[\frac{a}{b+I_s}-1\right]^2(1+\alpha^2)+2\alpha\omega I_s\left[\frac{a}{b+I_s}-1\right]+I_s\omega^2, \tag{10}$$

$$\omega=\frac{\rho}{\sqrt{I_s}}\sqrt{1+\alpha^2}\,\sin[\phi_s+\arctan(\alpha)]. \tag{11}$$

We consider henceforth the case $a>b$ (corresponding to the lasing mode of operation $\Gamma>\kappa$). For given (ρ,ω), the third degree-polynomial equation (10) can have either one or three real (always non-negative) solutions for the intensity I_s. For any of those solutions it is straightforward to show that the condition

$$|\omega|\leq\frac{\rho}{\sqrt{I_s}}\sqrt{1+\alpha^2} \tag{12}$$

is always satisfied, hence ensuring that there will be the corresponding solution for ϕ_s obtained from Eq. (11).

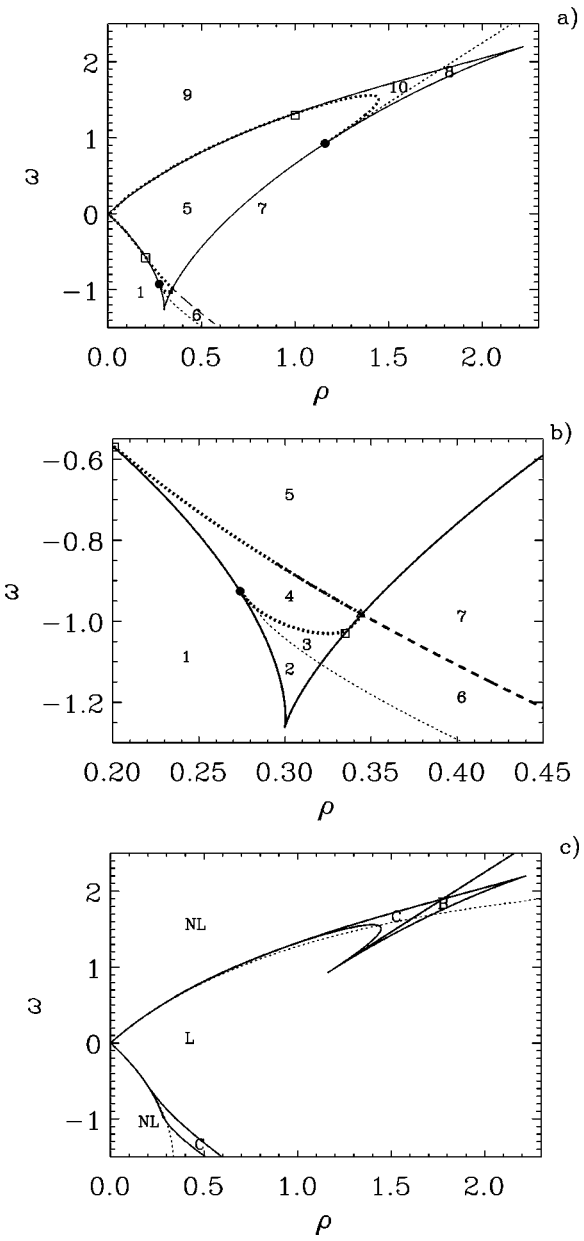

FIG. 1. Bifurcation set for a class-*A* laser with an injected signal for $a=2$, $b=1$, and $\alpha=2$. In (a) and (b) the solid line is the saddle-node curve separating regions 1, 6, 7, 9 with one fixed point solution from regions 2, 3, 4, 5, 8, 10 with three fixed point solutions; the short-dashed lines separating the pairs of regions 8-10; 2-3; 7-9; and 1-6, are Hopf bifurcations, as given by Eq. (20), where a periodic orbit is created; the dotted lines are homoclinic bifurcations where the periodic orbits of regions 4 and 10 disappear when going to region 5, and one periodic orbit in region 3 disappears when going to region 4; the coincidence of the curve of homoclinic orbits with the saddle-node curve mark the existence of Andronov-Leontovich bifurcations where the periodic orbit of regions 9 and 1 disappears when crossing to 5; the dashed line is a saddle node of periodic orbits and going from region 7 to 6 two periodic orbits of different stability are created; the two big solid dots are Takens-Bogdanov points. There exist also homoclinic saddle-node codimension-2 points, in the intersection between the saddle-node curves and the homoclinic orbits (squares and triangle). In (c) we indicate the different regions of stability: in *L*, one fixed point is the stable solution; in *NL*, one periodic orbit is the stable solution; in *C* there is coexistence of a stable fixed point and a periodic orbit; finally, in *B* there are two stable fixed points. The dotted line is the approximate locking range given by Eq. (18). Dimensionless units.

The lines separating the one fixed point solution region from the three fixed point solutions region can be found by using standard methods of algebra. These lines form the so-called *saddle-node* curve. It turns out that the three fixed points region is a connected set enclosing regions labeled 2, 3, 4, 5, 8, 10 shown in Fig. 1(a) for a typical case $a=2$, $b=1$, and $\alpha=2$. In regions 1, 6, 7, 9 only one fixed point is present. For moderate values of the intensity ρ, there is a range of values for the frequency $\omega\in(\omega_1,\omega_2)$ for which three fixed points exist, whereas for very large intensity, only one fixed point is present for all values of ω. A similar scenario occurs for $\alpha=0$, see Fig. 2 where the three fixed points region is labeled as 5, and only one fixed point appears in regions 1, 7, 9.

B. The periodic orbit solutions

At the saddle-node curve, a saddle point and another fixed point merge and disappear. In some cases this gives rise to a periodic orbit through an Andronov-Leontovich bifurcation. Near the bifurcation, it is possible to obtain approximately the evolution equation for the angle variable $\phi(t)$ by assuming that the intensity of the periodic orbit is constant. This approximation, which can be obtained via perturbation theory on the laser equations to lowest order [18], is derived here heuristically by neglecting fluctuations in the intensity, setting $\dot{I}=0$ in Eq. (8), but allowing for a time-dependent phase in Eq. (9) for ϕ. Setting $I=I_0$ constant in Eq. (8) and replacing in Eq. (9) we obtain

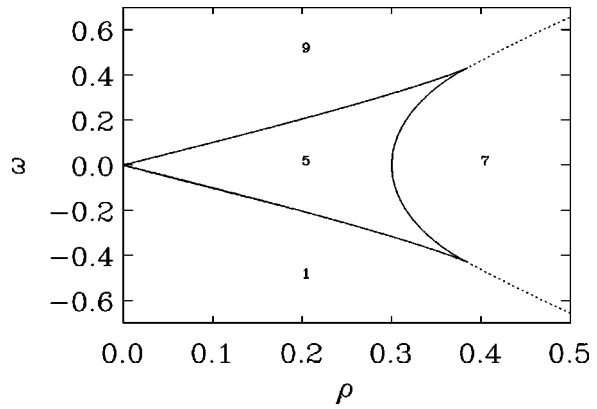

FIG. 2. Bifurcation set for a class-*A* laser with an injected signal for $a=2$, $b=1$, and $\alpha=0$. The solid line is the saddle-node curve separating regions 1, 7, 9 with one fixed point solution from region 5 with three fixed point solutions. The dotted lines separating the pairs of regions 7-9 and 7-1 are Hopf bifurcations, as given by Eq. (20), where a periodic orbit is created. The locking range is formed by regions 5, 7 where a single fixed point is the only stable solution. In regions 1 and 9 the stable solution is a periodic orbit. Dimensionless units.

$$\dot{\phi}=\omega-\frac{\rho\sqrt{1+\alpha^2}}{\sqrt{I_0}}\sin[\phi+\arctan(\alpha)]. \tag{13}$$

The next approximation is to consider that I_0 is the intensity of the field at the nearest point (ρ,ω) in the saddle-node curve with the same value of the external field amplitude ρ. Hence, I_0 is computed as the double root of Eq. (10) taking $\omega=\omega_1$ or $\omega=\omega_2$.

Equation (13) is known as Adler's equation [19] and it can be easily analyzed by writing it as

$$\dot{\phi}=-\frac{dU}{d\phi}, \tag{14}$$

using the potential function

$$U(\phi)=-\omega_L\cos[\phi+\arctan(\alpha)]-\omega\phi, \tag{15}$$

where we have introduced

$$\omega_L=\frac{\rho\sqrt{1+\alpha^2}}{\sqrt{I_0}}. \tag{16}$$

The dynamics of ϕ can then be explained in terms of relaxation in the potential U. For $|\omega|<\omega_L$ the potential has local minima and the phase eventually stops in one of them. This is a fixed point solution that has been discussed in the preceding subsection. A periodic orbit solution is obtained only in the case $|\omega|\geqslant\omega_L$ where the phase ϕ varies monotonically with time. The explicit solution is

$$\phi(t)=2\arctan\left[\frac{\omega_{ef}}{\omega}\tan\left(\frac{\omega_{ef}}{2}t\right)+\frac{\omega_L}{\omega}\right]-\arctan(\alpha)-\omega t, \tag{17}$$

where $\omega_{ef}=\sqrt{\omega^2-\omega_L^2}$.

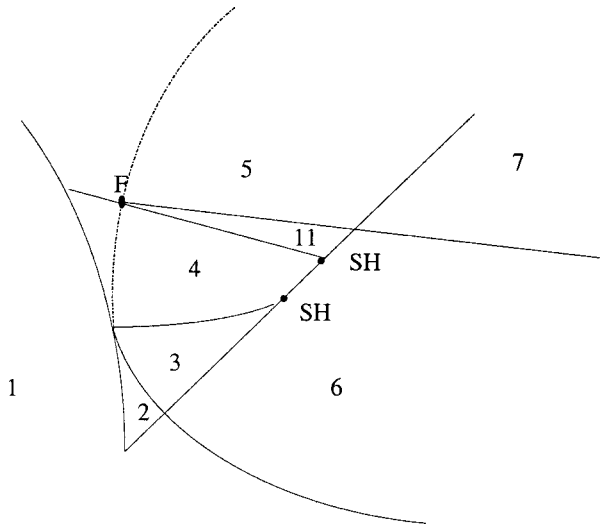

FIG. 3. Sketch of the partial bifurcation set for a class-*A* laser with injected signal $a=2$, $b=1$, and $\alpha=2$. Different regions and intersection points detailed in Fig. 1 and Table I. SH stands for homoclinic saddle-node codimension-2 points. F stands for intersection of the saddle-node bifurcation of periodic orbits, the homoclinic orbit, and the continuation of the Hopf bifurcation (dotted line, which is not a bifurcation). Dimensionless units.

Therefore, within this approximation, the line separating a fixed point from a periodic orbit solution is given by $|\omega|=\omega_L$. Notice that our derivation of this relation is different from the usual one in which one derives it by demanding that Eq. (12) can be satisfied. We have shown that Eq. (12) is indeed satisfied for all values of ω and ρ and that the condition $|\omega|=\omega_L$ to determine the locking range is an approximate one. By using Eq. (10) this condition can be rewritten as

$$\rho=|\omega|\sqrt{\frac{a}{1+\alpha^2-\alpha\omega}-\frac{b}{1+\alpha^2}}\ . \tag{18}$$

The range of validity of this approximation has to be checked numerically. In Fig. 1(c) we compare the exact result with the approximate one in the typical case $a=2$, $b=1$, and $\alpha=2$. It can be seen that the approximation is quite good for small values of ρ but it worsens as the intensity ρ is increased.

When crossing the saddle-node curve, for example, crossing from region 9 or 1 to region 5 in Fig. 1(a), the periodic orbit disappears. As a precursor of this disappearance, the period of the periodic orbit, T, grows in regions 1, 9 until it finally diverges at the saddle-node curve. The divergence can be fitted, for a fixed value of ω to the law $T\sim(\rho_r-\rho)^{-1/2}$ [20], with ρ_r the value of ρ where the bifurcation occurs.

C. The bifurcation set

In the following we will perform the stability analysis of the different fixed point and periodic orbit solutions. The fixed points for I are given by Eq. (10) and this equation can

have either one or three real roots depending on ρ and ω. The stability of these fixed points defines the different regions of interest. Stability properties can be established in terms of the eigenvalues of the linearization matrix (Jacobian) of Eqs. (6),(7) at the fixed points. A fixed point is stable if both eigenvalues have a negative real part. We will call a fixed point unstable if both eigenvalues have positive real part, while a saddle fixed point will be characterized by having one eigenvalue with positive real part and the other with negative real part. The local bifurcation takes place when the real part of some eigenvalue crosses zero.

The results of the stability analysis depend on the value of the parameter α. For $\alpha=0$, the only possibility is to have regions in which either a stable fixed point or a stable periodic orbit exist, see Fig. 2. However, for $\alpha>0$ a much richer behavior appears. We summarize the results for one interesting typical case, namely $a=2$, $b=1$, and $\alpha=2$, shown in Fig. 1. In regions 5, 7 there exists only one locking (stable fixed point) solution. In region 8 there exist two locking solutions with different intensity. In regions 1, 2, 9 there exists one stable periodic orbit solution. Finally, in regions 3, 4, 6, 10, and 11 (appearing in Fig. 3) one locking solution coexists with a stable periodic orbit solution. While some of the lines of this bifurcation set shown in Fig. 1 can be evaluated analytically, others have to be obtained numerically. We now give details of the calculations of those lines. The reader not interested in the technical details can skip directly to Sec. III C 6.

1. Saddle-node bifurcation

A saddle-node bifurcation occurs when two fixed points are created/annihilated. The saddle-node curve separates, in this case, a region with one fixed point from another with three fixed points. On the saddle-node curve, two fixed points coincide (or equivalently, one of the eigenvalues of the Jacobian is zero). From another point of view, the saddle-node bifurcation curve can be obtained as the lines in the (ρ,ω) plane in which the third degree equation (10) has a double root. The saddle–node bifurcation curve is indicated by a solid line in Figs. 1(a), 1(b), and 2.

2. Hopf bifurcation

In a Hopf bifurcation of a two-dimensional system such as ours, a fixed point changes its stability (from stable to unstable, or vice versa) and a periodic orbit with opposite stability to the coexistent fixed point is born/disappears. At the bifurcation point, the eigenvalues of the Jacobian matrix J associated with the deterministic system (6) and (7) [or, equivalently and somewhat easier, (8) and (9)] are complex conjugated and pure imaginary. This condition can be written as $\mathrm{Tr}(J)=0, \quad \mathrm{Det}(J)>0$. Hence,

$$(b+I)(a-b-I)-aI=0. \tag{19}$$

This equation combined with the one for the fixed points (10) leads to the Hopf bifurcation curve,

$$\omega^2+2\alpha\omega\left(\sqrt{\frac{a}{b}}-1\right)+\left(\sqrt{\frac{a}{b}}-1\right)^2(1+\alpha^2)=\frac{\rho^2}{-b+\sqrt{ba}}. \tag{20}$$

The resulting Hopf bifurcation is also shown in Figs. 1(a) and 1(b) (short-dashed line). From regions 8 to 10 and from 2 to 3 a periodic orbit is born and a fixed point changes its stability. The disappearance of those periodic orbits will be explained in the following subsections.

3. Takens-Bogdanov singularities

At the points (ρ_{Hs},ω_{Hs}) where the Hopf and the saddle-node bifurcation curves intersect, the eigenvalues of the Jacobian matrix are strictly equal to zero. This condition gives

$$\omega_{Hs}=\pm\left(\sqrt{\frac{a}{b}}-1\right)\sqrt{1+\alpha^2}, \tag{21}$$

$$\rho_{Hs}=\sqrt{2b\left(\sqrt{\frac{a}{b}}-1\right)^3\sqrt{1+\alpha^2}\left(\sqrt{1+\alpha^2}\pm\alpha\right)}. \tag{22}$$

For the parameters considered in Fig. 1 ($a=2$, $b=1$, and $\alpha=2$), it is $(\rho_{Hs},\omega_{Hs})=(0.274,-0.926)$ and $(\rho_{Hs},\omega_{Hs})=(1.160,0.926)$. At these intersection points, the Jacobian matrix is different from zero, and its normal form is

$$\begin{pmatrix}0 & 1\\ 0 & 0\end{pmatrix}. \tag{23}$$

These points correspond to Takens-Bogdanov singularities [21]. At these codimension-3 points, indicated in the figure, a homoclinic orbit is also born. These orbits have been computed numerically and they are discussed in the following subsection.

4. Homoclinic orbits

When (some branch of) the stable and unstable manifolds of a saddle point coincide we are in the presence of a homoclinic orbit. Homoclinic orbits have been obtained numerically using the program AUTO97 [22] as the ''infinite-

TABLE I. Different regions in the bifurcation set for a class-*A* laser with injected signal. fp stands for fixed point, po stands for periodic orbit, St. stands for stable, and Unst. stands for unstable.

1→	1 fp Unst., 1 po St.
2→	2 fp Unst., 1 fp Saddle, 1 po St.
3→	1 fp Unst., 1 fp Saddle, 1 fp St., 1 po St., 1 po Unst.
4→	1 fp Unst., 1 fp Saddle, 1 fp St., 1 po St.
5→	1 fp Unst., 1 fp Saddle, 1 fp St.
6→	1 fp St., 1 po St., 1 po Unst.
7→	1 fp St.
8→	2 fp St., 1 fp Saddle
9→	1 fp Unst., 1 po St.
10→	1 fp Unst., 1 fp Saddle, 1 fp St., 1 po St.
11→	1 fp Unst., 1 fp Saddle, 1 fp St., 1 po St., 1 po Unst.

period limit'' of periodic orbits. The resulting curves of homoclinic orbits are displayed as dotted lines in Figs. 1(a) and 1(b). Their location in parameter space coincides partially with the saddle-node curve.

The intersections of the saddle-node curve and a homoclinic bifurcation occur at codimension-2 points. There exist intersection homoclinic saddle-node codimension-2 points (SH) at each of the saddle-node branches, see Figs. 1 and 3. The bifurcation structure near to these points was described in Ref. [23]. Note that the location of these codimension-2 points cannot be completely exact due to the fact that the homoclinic orbits are obtained numerically. The bifurcation branch emerging from these points with coincidence of the curve of homoclinic orbits with the saddle-node curve is called the Andronov-Leontovich bifurcation [24], or more generally called *saddle-node bifurcation on a limit cycle* or *saddle-node infinite period bifurcation* [20].

5. Saddle-node of periodic orbits

Besides the bifurcation curves described so far, there exists yet another curve of saddle-node bifurcations of periodic orbits. This is indicated by the the long-dashed curve in Figs. 1(a) and 1(b), which has been obtained also numerically. When crossing this curve, the two periodic orbits of region 6 disappear. The point were the saddle-node of periodic orbits, the homoclinic and the neutral saddle curve intersect is a codimension-2 point, labeled as *F*, [21], in Fig. 3. This point is not found exactly at Fig. 1(b) due to numerical evaluation. The presence of this point gives rise to a small region, labeled as 11, where two periodic orbits, and three fixed points exist, see Figs. 3 and 6. For $\omega \approx -5$ [not shown in the scale of Fig. 1(a)] the Hopf bifurcation and the saddle-node of periodic orbits collide and regions 1 and 7 are directly separated by the Hopf bifurcation, this kind of bifurcation appears in other systems, as in Ref. [25].

6. Summary

We summarize in Table I the results of the previous subsections concerning the different regions separated by the bifurcation lines. In Fig. 4, the phase portrait of different regions is shown, namely, regions 3, 4, 5, 6. In the first line,

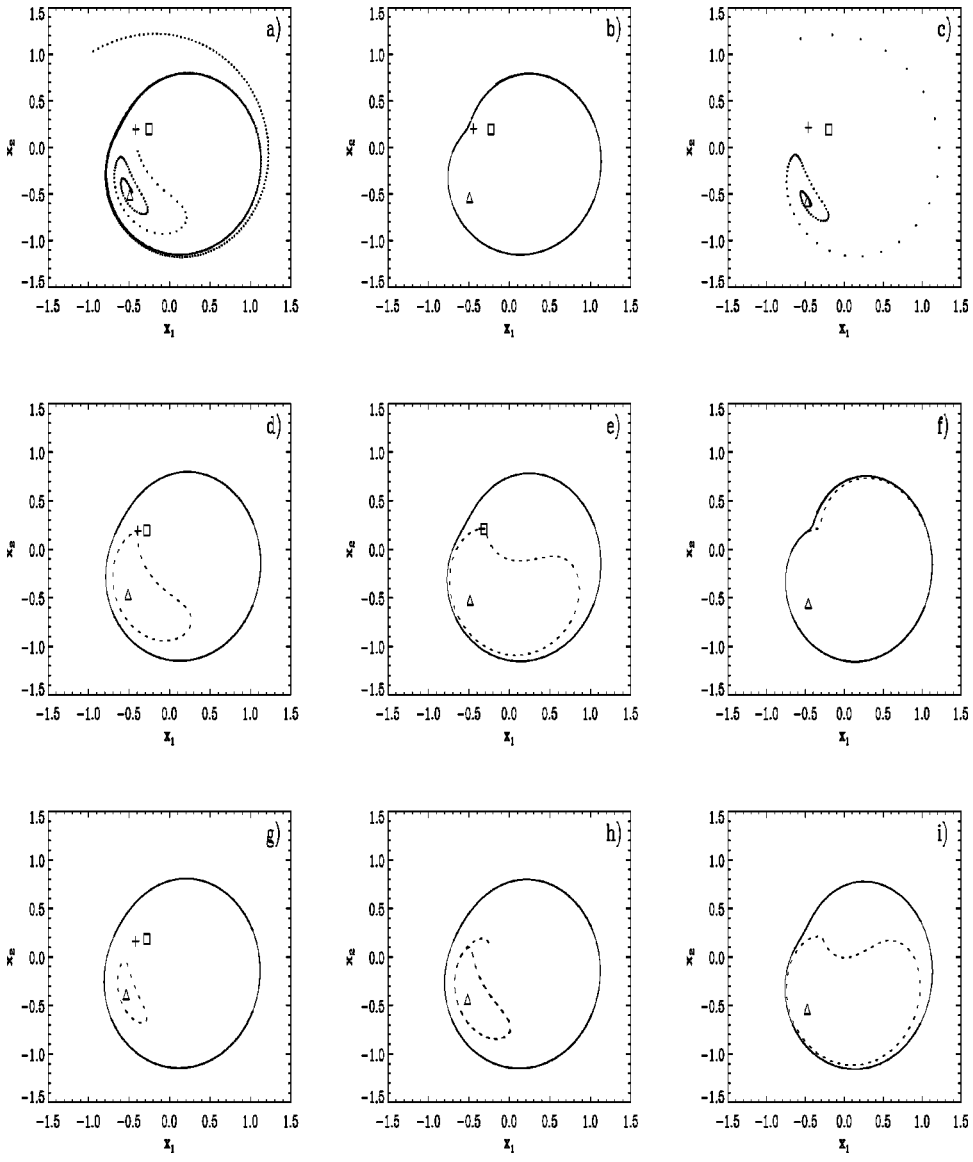

FIG. 4. Phase portraits (x_1, x_2) in different regions. Dimensionless units. Triangle, stable fixed point; square, unstable fixed point; cross, saddle point. Solid line, stable orbit; dashed line, unstable orbit; points, trajectories. (a) Region 4, $(\rho,\omega)=(0.33,-1)$; (b) near homoclinic 4, 5, $(\rho,\omega)=(0.33,-0.95)$; (c) region 5, $(\rho,\omega)=(0.33,-0.9)$; (d) close to homoclinic 3, 4, $(\rho,\omega)=(0.33,-1.03)$; (e) close to Andronov bifurcation 4, 6, $(\rho,\omega)=(0.34,-1)$; (f) close to the saddle node of periodic orbits 6, 7, $(\rho,\omega)=(0.352,-1)$; (g) region 3, $(\rho,\omega)=(0.32,-1.07)$; (h) close to the saddle node 3, 6, $(\rho,\omega)=(0.33-1.065,)$; (i) region 6, $(\rho,\omega)=(0.345,-1)$.

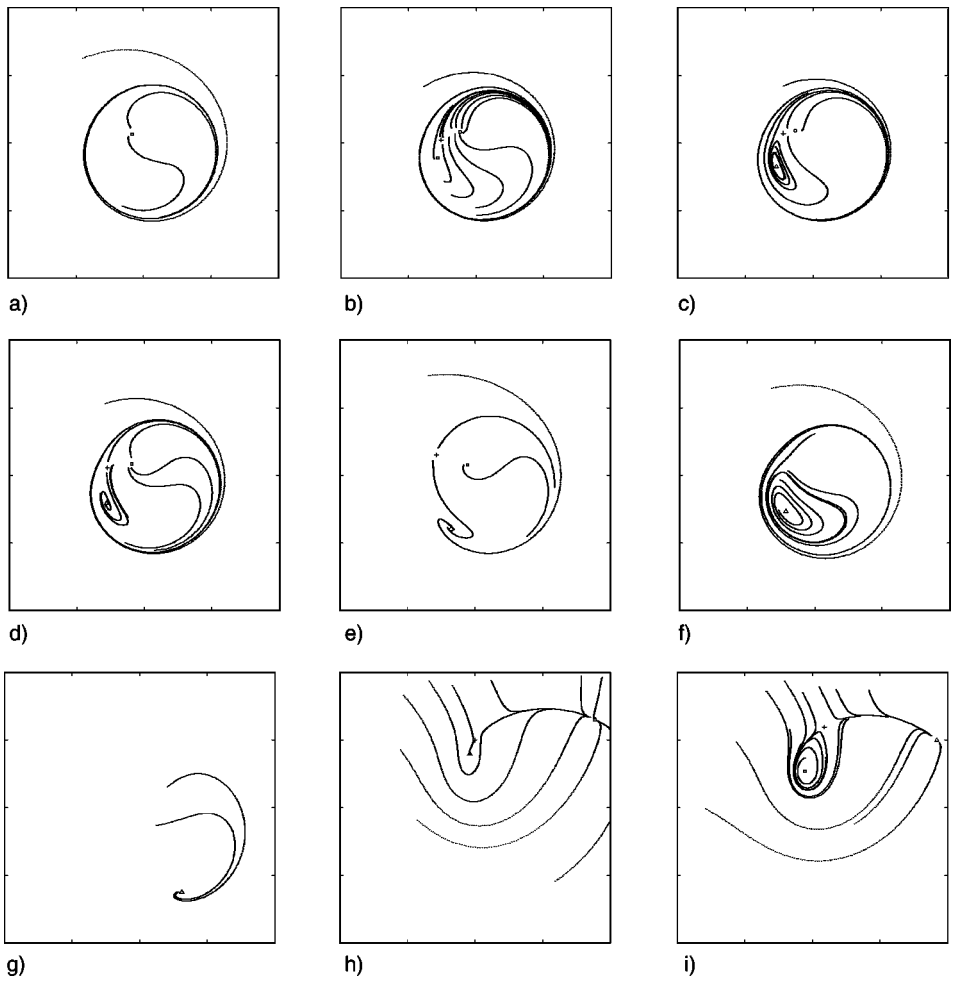

FIG. 5. Phase portraits (x_1, x_2) in different regions of the bifurcation set. Dimensionless units. Triangle, stable fixed point; square, unstable fixed point; cross, saddle point. (a) region 1, $(\rho,\omega)=(0.25, -1.1)$; (b) region 2, $(\rho,\omega)=(0.3,-1.1)$; (c) region 3, $(\rho,\omega)=(0.315,-1.08)$; (d) region 4, $(\rho,\omega)=(0.3,-0.95)$; (e) region 5, $(\rho,\omega)=(0.3,-0.6)$; (f) region 6, $(\rho,\omega)=(0.4,-1.2)$; (g) region 7, $(\rho,\omega)=(1,0)$; (h) region 8, $(\rho,\omega)=(1.8,1.8)$; (i) region 10, $(\rho,\omega)=(1.5,1.6)$.

from left to right the transition from region 4 to 5 is shown. In the first column, one can observe the transition form region 4 to 3 through an homoclinic orbit. The transition from region 3 to 6, as a saddle-node bifurcation, appears in the last line. In the diagonal [Figs. 4(a), 4(e) and 4(i)] one can observe the transition through an Andronov bifurcation. The saddle-node of periodic orbits is reflected in Fig. 4(f). In Figs. 5 and 6, there appear the phase portraits of the different regions obtained, region 11 has also been sketched to make a more representative plot.

Many of the bifurcation features found in this system are present in other studies, we mention in particular the paper by Khibnik *et al.* [25,26] and more importantly the book by Kuznetsov [21] where a bifurcation diagram topologically equivalent to ours is displayed in Fig. 8.10, p. 285 in connection with the analysis of a predator-prey model by Bazykin.

These results allow us to identify the stability regions indicated in Fig. 1(c): in **L**, one fixed point is the only stable solution; in **NL**, one periodic orbit is the only stable solution; in **C** there is coexistence of a stable fixed point and a periodic orbit; finally, in **B** there are two stable fixed points.

7. Comparison with the bifurcation set for class-B lasers

The bifurcation set obtained in the previous analysis reveals the complexity of the system and the importance of the parameter choice in experiments. Class-*A* lasers with injected signal are the simplest example one can consider. A more complex situation arises when considering class-*B* [3,27–31] lasers with injected signal (described with equations for the electric field and carriers number). The main difference between class-*A* and class-*B* lasers from the dynamical point of view is the number of variables that one works with. For class-*A* lasers two variables suffice and the full bifurcation set can be described. For class-*B* lasers, a three-dimensional system, a more complex variety of phenomena can appear and the system can also show chaotic behavior. Although part of the bifurcation structure of class-*B* lasers is already present in class-*A* lasers (essentially the three curves of saddle-node bifurcations of fixed points), the overall dynamics of the former becomes extremely complicated. The presence of the Hopf-saddle-node point has a crucial importance for class-*B* lasers and different types of flows (as classified by Ref. [10]) can be obtained. The analysis of these flows has been the object of a extensive work: type III [32], type I [18], and type II [24] of the Hopf–saddle-node singularity occur for different parameter regions. Note as contrast that the intersection of Hopf and saddle-node bifurcations of fixed points in class *A* cannot be of Hopf–saddle-node type but are Takens-Bogdanov singularities instead. Such singularities are, however, also present (in a different form) in class *B*, not only involving bifurcation of fixed

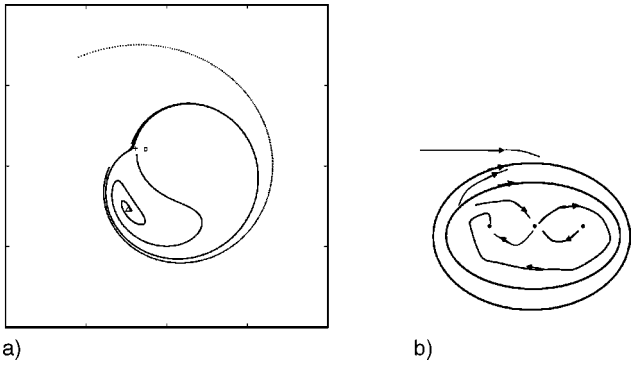

FIG. 6. Phase portrait at region 11 of the bifurcation set. (a) $(\rho,\omega)=(0.34,-0.9713)$; triangle, stable fixed point; square, unstable fixed point; cross, saddle point. (b) Sketch of the phase portrait: arrows indicate the sense of the flow. Dimensionless units.

points but also bifurcations of periodic orbits. Andronov global bifurcations have also been found in both types of lasers. In the bifurcation set for a class-*A* laser in the case $\alpha=2$ several changes (codimension-3 bifurcations) would need to take place to get it from the $\alpha=0$ situation (Fig. 2), this situation is again reminiscent of the class-*B* laser case [33].

IV. LYAPUNOV POTENTIAL

We now look for a description of the dynamical equations in terms of a Lyapunov potential [10]. Equations (6),(7) can be written as

$$\dot{x}_i=-\sum_{j=1}^{2} D_{ij}\frac{\partial V}{\partial x_j}+v_i+\sum_{j=1}^{2} g_{ij}\xi_j, \quad i=1,2, \tag{24}$$

where the function V is [34]

$$V(x_1,x_2)=\frac{1}{2}[x_1^2+x_2^2-a\ln(b+x_1^2+x_2^2)]$$

$$-\frac{\rho}{(1+\alpha^2)}(x_1-\alpha x_2), \tag{25}$$

or, written in terms of intensity and phase,

$$V(I,\phi)=\frac{1}{2}[I-a\ln(b+I)]-\frac{\rho\sqrt{I}}{\sqrt{1+\alpha^2}}\cos(\phi+\arctan\alpha). \tag{26}$$

The matrices **D** and **g**, and the vector **v** are

$$\mathbf{D}=\mathbf{S}+\mathbf{A}=\begin{pmatrix}1 & 0\\ 0 & 1\end{pmatrix}+\begin{pmatrix}0 & -\alpha\\ \alpha & 0\end{pmatrix}, \quad \mathbf{g}=\begin{pmatrix}1 & 0\\ 0 & 1\end{pmatrix},$$

$$\mathbf{v}=\begin{pmatrix}-\omega x_2\\ \omega x_1\end{pmatrix}. \tag{27}$$

A. Deterministic dynamics

In the deterministic dynamics ($\epsilon=0$), Eqs. (24) show that $V(x_1,x_2)$ is a Lyapunov potential, i.e., a function that monotonically decreases along trajectories, $\dot{V}\leqslant 0$, provided that the *residual terms* (v_1,v_2) satisfy the *orthogonality condition* [35]

$$v_1\frac{\partial V}{\partial x_1}+v_2\frac{\partial V}{\partial x_2}=0. \tag{28}$$

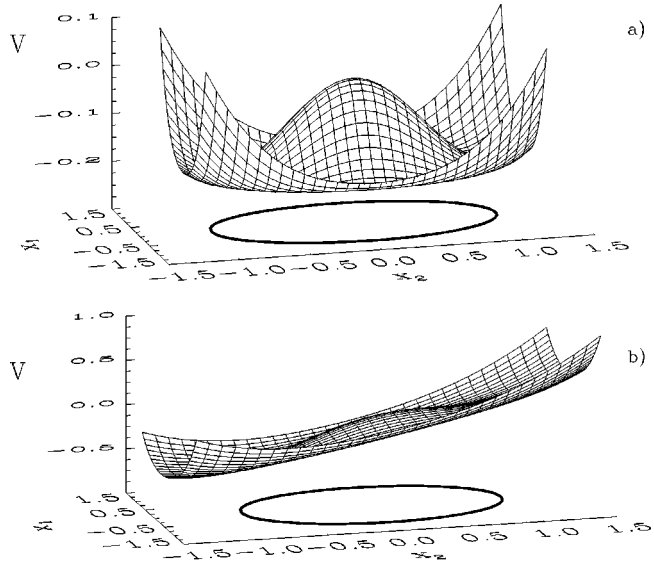

FIG. 7. Potential for a class-*A* laser with an injected signal with the same frequency of the unperturbed laser, Eq. (25), with the parameters $a=2$, $b=1$, and $\alpha=2$. Dimensionless units. (a) $\rho=0$, (b) $\rho=0.8$. In (a) we also indicate the projection of the line of minima of V and the corresponding line is plotted in (b).

It turns out that this orthogonality condition is satisfied if $\omega\rho=0$. This means that a Lyapunov function description of the dynamics using Eq. (25) is valid along the coordinate axis $\omega=0$ and $\rho=0$. Notice that the case $\rho=0$, $\omega\neq 0$ corresponds to a situation in which there is no applied field but the reference system rotates at an arbitrary frequency ω.

The use of a Lyapunov function potential permits to visualize the dynamics as the relaxation of a fictitious test particle in the potential landscape. The fixed points of the deterministic dynamics can be regarded as the extrema of the potential V, where minima correspond to stable fixed points, maxima correspond to unstable fixed points, and saddle extrema correspond to saddle points. In the transient dynamics towards the stationary states, the symmetric matrix **S** is responsible for driving the system towards the minimum of V following the lines of maximum slope of V. The antisymmetric part **A** (which is proportional to α) induces a movement orthogonal to the direction of maximum variation of V. The combined effects of **S** and **A** produce in general a spiral-like trajectory in the (x_1,x_2) plane. The angular velocity of this movement is proportional to α. Finally, the residual term (v_1,v_2) induces a movement that does not decrease the value of the potential and it is responsible for any dynamics after the line of minima of the potential has been reached. We now analyze the different possibilities for the extrema of V.

In the case $\rho=0$, the potential does not depend on the phase ϕ of the electric field and it can adopt two qualitatively different shapes.

(i) For $a<b$ the potential has a single minimum at $x_1=x_2=0$ and no maxima. Therefore, the only fixed point is the *off* state $I=0$, which is stable.

(ii) For $a>b$, the potential has the shape of a sombrero, see Fig. 7(a). There is a single maximum at $(x_1,x_2)=0$ (corresponding to the unstable situation with the laser in the *off* state) and a circumference of degenerate minima at $x_1^2+x_2^2=a-b$. The asymptotically stable situation, then, is that the laser switches to the *on* state with intensity $I_{st}=(x_1^2+x_2^2)_{st}=a-b$ and arbitrary phase. The residual dynamics $\dot{x}_i=v_i$ gives a periodic harmonic movement in the minima of the potential with frequency ω. This corresponds to the periodic orbits shown in Fig. 1.

In the case of zero-detuning injected signal, $\rho>0$, $\omega=0$, the potential, which depends now explicitly on the phase ϕ, is tilted in a preferred direction. In the case $a<b$ the location of the only minimum changes and the asymptotic state has a nonzero light intensity, proportional to ρ. In the case $a>b$, the sombrero is tilted as well in a preferred direction. For small ρ the inclination is small and the effect is that the maximum still remains a maximum, although its location varies accordingly. The tilt breaks the symmetry amongst the line of degenerate minima and an absolute minimum is selected. At the same time, one of the previous minima becomes a maximum in the direction orthogonal to the tilt and a saddle point is born. Increasing ρ, the maximum of the sombrero and the saddle point disappear (corresponding to the saddle-node curve of Fig. 1) and the potential has only one minimum at a preferred phase direction, see Fig. 7(b). Therefore, the asymptotically stable situation, in this case of $\rho>0$, $\omega=0$ and $a>b$ is that the laser switches to an *on* state with a well defined intensity and phase, in agreement with the results shown in Fig. 1.

The validity of a Lyapunov potential description in the general case, $\rho\omega\neq 0$ is an open question. Since the orthogonality condition implies that the time derivative of the Lyapunov functional (25) has a negative contribution plus an extra term proportional to $\omega\rho$ (with no definite sign), it is reasonable to speculate that for $\omega\rho$ small enough, the latter term can be compensated by a change of the same order in the potential. However, we have not been able to find an analytical expression for the potential V in this general case. This speculation is supported by the fact that the *qualitative* dynamical features do not change near the coordinate axis $\omega=0$, $\rho=0$. Furthermore, assuming the validity of this Lyapunov potential description we can understand the transition from locking to nonlocking states.

Let us consider a given value of $\rho>0$ and increase the detuning frequency starting from $\omega=0$. For $\omega=0$, the potential is tilted and there are no residual terms [see Fig. 7(b)]. As ω increases, the shape of the potential deforms, the minimum of the potential and the saddle point approach through the deterministic noninjection circumference of minima (region 5 of Fig. 1). Moreover, the residual terms, proportional to ω increase, but still they are not strong enough to overcome the tilt of the potential and to induce a rotation movement. For a value of ω (corresponding to the saddle-node bifurcation) these two points (minimum and saddle) collapse and a periodic motion appears, induced by the residual terms (corresponding to region 9 of Fig. 1).

Similarly, starting at a point $\omega>0$ and increasing the intensity of the applied fields, ρ, a similar scenario appears. For $\rho=0$, the potential has a line of degenerate minima, $I=a-b$, and trajectories are circumferences in the (x_1,x_2) plane induced by the residual terms. Increasing ρ, the line of minima deviate from the circumference due to the change of shape of the potential and it becomes an ellipse, the periodic orbit solution is also induced by the residual terms of the dynamics, which are proportional to ω. In fact, it can be shown that the solution in the steady state for very small values of ρ has the form

$$I(t)=\frac{a-b}{1-e\cos[\phi(t)+\delta]}, \tag{29}$$

which represents an ellipse with a time dependent time phase. The explicit values of e and δ can be obtained in terms of the laser parameters from Eqs. (8) and (9) and for small values of ρ. Increasing ρ even further, the potential deforms continuously until arriving to the saddle–node bifurcation.

B. Stochastic effects

In the presence of moderate levels of noise, $\epsilon>0$, the qualitative features of the transient dynamics remain the same as in the deterministic case. The most important differences appear near the stationary situation and show up as fluctuations of the intensity and phase of the electric field. While the intensity simply oscillates around its mean value, one can observe in some cases an additional phase drift that shows up as a variation in the frequency of the emitted light. The potential picture developed in the preceding section helps us to understand the origin of this noise-induced frequency shift, as well as to compute its magnitude.

Let us look at the potentials depicted in Fig. 7. First consider the case $\rho=0$. The deterministic movement is such that the line of minima [shown as a projection in the (x_1,x_2) plane] is run at a constant frequency ω. On top of that movement there are fluctuations that allow frequent excursions beyond the minima of the potential V. When away from the minima, the antisymmetric part of the dynamics [governed by the matrix **A** in Eq. (27) and proportional to α] gives a nonzero contribution of the rotation terms producing the phase drift observed. For $\omega=0$, $\rho\neq 0$, when there exists just one minimum of the potential, the fluctuations allow the system to explore regions outside this minimum and then the rotation terms act again. Depending on the value of ρ and ϵ the rotation term can be strong enough to produce the phase flow or not.

After these qualitative arguments, we now turn to a more quantitative calculation. In those cases that there exists a Lyapunov potential $V(x_1,x_2)$ and that the matrices **S** and **g**

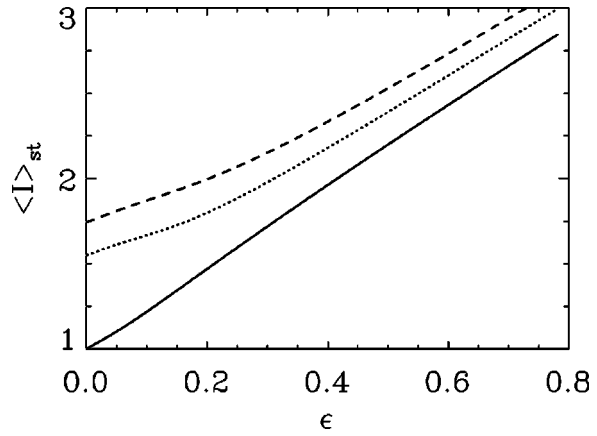

FIG. 8. Mean value of the intensity in the steady state in a class-*A* laser with zero-detuning injected signal for $a=2$, $b=1$, and $\alpha=2$. Dimensionless units. The solid line corresponds to $\rho=0$ and has been computed using the analytical result Eq. (33), the dotted line ($\rho=0.6$) and the dashed line ($\rho=0.8$) have been computed numerically using Eq. (32).

of Eq. (24) satisfy the fluctuation-dissipation relation $\mathbf{S}=\mathbf{g}\mathbf{g}^{\top}$, Graham [36] has shown that the stationary probability distribution is given by

$$P_{st}(x_1,x_2)=Z^{-1}\exp\left(-\frac{V(x_1,x_2)}{\epsilon}\right), \tag{30}$$

where Z is a normalization constant. This relation is exact if the residual terms $\mathbf{v}$ satisfy the orthogonality condition (28) and if they are divergence free: $\partial_{x_1}v_1+\partial_{x_2}v_2=0$ (as they are in our case). In other cases, it has to be understood as an approximation valid in the limit of small noise $\epsilon\to 0$.

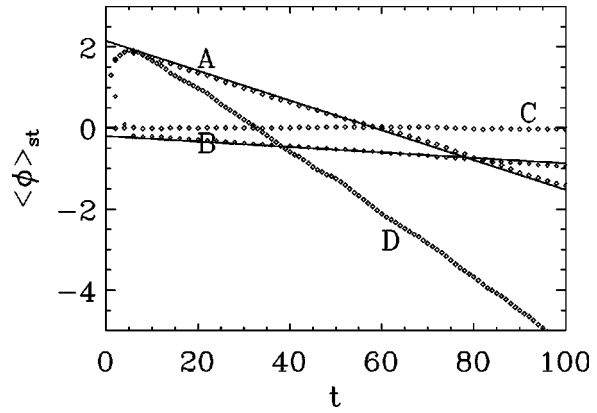

FIG. 9. Time evolution of the mean value of the phase ϕ in a class-*A* laser without injected signal $\rho=0$ (line *A*) and zero-detuning injected signal $\rho=0.6$ (line *B*), in the case $\alpha=2$ there is a linear variation of the mean value of the phase at late times. For $\alpha=0$ (line *C*) there is only phase diffusion and the average value is 0 for all times. The solid lines have the slope given by the theoretical prediction Eq. (35). Line *D*, time evolution of $\langle\phi\rangle_{st}-2\pi t/T$, T being the period of the periodic orbit in the deterministic case, for $\rho=0.5$, $\omega=1$. In all the curves: $a=2$, $b=1$, and $\epsilon=0.1$. Dimensionless units.

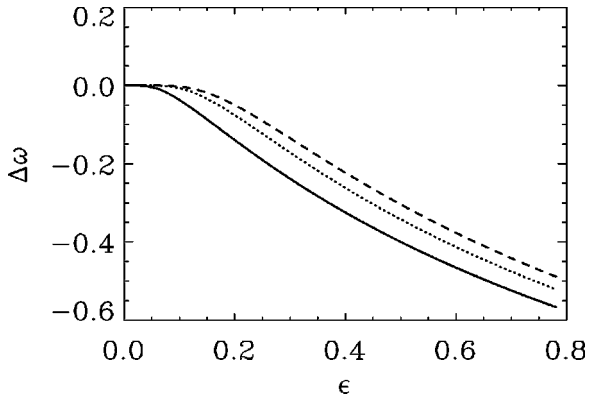

FIG. 10. Stochastic frequency shift $\Delta\omega\equiv\langle\dot{\phi}\rangle$ in a class-*A* laser for $a=2$, $b=1$, and $\alpha=2$. For $\rho=0$ (solid line) the explicit result Eq. (35) is used, whereas for $\rho=0.6$ (dotted line) and $\rho=0.8$ (dashed line) Eq. (34) has been evaluated numerically. Dimensionless units.

By changing variables to intensity and phase, we find that the probability density function is

$$P_{st}(I,\phi)=Z^{-1}e^{-I/2\epsilon}(b+I)^{a/2\epsilon}\times\exp\left(\frac{\rho\sqrt{I}}{\epsilon\sqrt{1+\alpha^2}}\cos(\phi+\arctan(\alpha))\right), \tag{31}$$

and the marginal probability density function for I is

$$P_{st}(I)=Z^{-1}e^{-I/2\epsilon}(b+I)^{a/2\epsilon}I_0\left(\frac{\rho\sqrt{I}}{\epsilon\sqrt{1+\alpha^2}}\right), \tag{32}$$

where I_k is the Bessel function of the first kind and order k. The steady-state average value for the intensity $\langle I\rangle_{st}=\int dI I P_{st}(I)$ can be analytically computed in the case $\rho=0$ with the result

$$\langle I\rangle_{st}=a-b+2\epsilon\left[1+\frac{e^{-b/2\epsilon}\left(\frac{b}{2\epsilon}\right)^{1+a/2\epsilon}}{\Gamma\left(1+\frac{a}{2\epsilon},\frac{b}{2\epsilon}\right)}\right]. \tag{33}$$

In the most general case, for $\rho\neq 0$, the mean value can be computed numerically by using Eq. (32). In Fig. 8, this mean value is represented, for fixed value of ρ, versus ϵ. The mean value is always larger than the deterministic ($\epsilon=0$) case.

As mentioned before, in the steady state of the stochastic dynamics, the phase ϕ of the electric field fluctuates around a mean value that changes linearly with time. This is clearly seen in the numerical simulations, see Fig. 9, and physically corresponds to a change $\Delta\omega$ in the emission frequency of the laser. This frequency shift can be computed as the average value of the phase derivative $\langle\dot{\phi}\rangle$. In the case that the steady

state is a periodic orbit of period T, one needs to subtract from this value the intrinsic frequency $2\pi/T$. By taking the average value of Eq. (9) and using the rules of the stochastic calculus, one arrives to

$$\Delta\omega = Z^{-1}\alpha\int_0^\infty e^{-I/2\epsilon}(b+I)^{a/2\epsilon}\left[\frac{(a-b-I)}{b+I}I_o\left(\frac{\rho\sqrt{I}}{\epsilon\sqrt{1+\alpha^2}}\right) + \sqrt{I}I_1\left(\frac{\rho\sqrt{I}}{\epsilon\sqrt{1+\alpha^2}}\right)\right]dI. \tag{34}$$

Notice that this stochastic frequency shift is zero in the case $\alpha=0$ or for the deterministic dynamics ($\epsilon=0$). In the case $\rho=0$ this expression can be analytically computed [9]

$$\Delta\omega = -\alpha\frac{e^{-b/2\epsilon}\left(\frac{b}{2\epsilon}\right)^{a/2\epsilon}}{\Gamma\left(1+\frac{a}{2\epsilon},\frac{b}{2\epsilon}\right)}. \tag{35}$$

For $\rho\neq 0$, one needs to compute the expression (34) numerically. In any case, the results are in excellent agreement with numerical simulations of the rate equations in the presence of noise. In Fig. 10, we plot the stochastic frequency shift as a function of the noise intensity for several values of ρ. For a fixed value of ρ, $|\Delta\omega|$ increases as ϵ increases, since a larger value of ϵ can induce larger fluctuations and larger excursions in phase space (x_1,x_2) away from the minima of the potential. For fixed ϵ, $|\Delta\omega|$ decreases as ρ increases. This is because when ρ is increased, the inclination of the potential increases, so the trajectory becomes more confined around a fixed value.

In the case $\rho\neq 0$ and $\omega\neq 0$, the stochastic frequency shift is also present, see Fig. 9 (line D), although it is not possible to compute its magnitude because we do not have an explicit expression for the Lyapunov potential.

V. CONCLUSIONS

In this work we have studied a class-*A* laser with an injected electrical field. By using analytical and numerical tools we have been able to describe the whole bifurcation set of this system and to determine the *locking range*, i.e., the set of amplitudes and (detuning) frequencies (ρ,ω) for which the laser responds adjusting its frequency to that of the external field. This result is summarized in Fig. 1(c) in which we can identify nonlocking regions (labeled NL in that figure). Within the locking range one finds a region with a single stable laser response (L), regions (C) of coexistence of a locking solution with a nonlocking solution, as well as a region (B) of coexistence of two locking solutions of different light intensity.

We have described qualitatively the observed features of the deterministic dynamics in terms of a Lyapunov potential landscape. We have identified the relaxational, conservative, and residual terms in the dynamical equations of motion. Although this description is strictly valid only in the case of a zero-detuning injected signal, the qualitative features remain unchanged when the product $\rho\omega$ is small.

In the stochastic dynamics (when the additive noise coming from the spontaneous emission is explicitly considered in the equations), we have used the Lyapunov potential image to explain the presence of a *stochastic frequency shift* of the laser light. The same potential allows a quantitative calculation of this effect. The results are in good agreement with numerical simulations of the model equations and we hope that they can be a guide for future experiments in observing this effect in real laser systems.

ACKNOWLEDGMENTS

Fruitful discussions with Martín Zimmermann, Hernán Solari, and Magnus Fontes are gratefully acknowledged. We wish to thank Bernd Krauskopf for a careful reading of this manuscript and useful comments. We acknowledge financial support from MCyT (Spain) projects BFM2001-0341-C02-01 and BMF2000-0624.

[1] J. R. Tredicce, G. L. Lippi, and G. P. Puccioni, J. Opt. Soc. Am. B **2**, 173 (1985).
[2] H. G. Solari and G. L. Oppo, Opt. Commun. **111**, 173 (1994).
[3] S. Wieczork, B. Krauskopf, and D. Lenstra, Opt. Commun. **172**, 279 (2000).
[4] T. Simpson, J. M. Liu, K. F. Huang, and K. Tai, Quantum Semiclassic. Opt. **9**, 765 (1997).
[5] H. Haken, *Laser Light Dynamics*, Light Vol. 2 (North-Holland, Amsterdam, 1985).
[6] F. T. Arecchi, G. L. Lippi, G. P. Puccioni, and J. R. Tredicce, Opt. Commun. **51**, 308 (1984).
[7] S. Ciuchi, F. de Pasquale, M. San Miguel, and N. B. Abraham, Phys. Rev. A **44**, 7657 (1991).
[8] E. Hernández-García, R. Toral, and M. San Miguel, Phys. Rev. A **42**, 6823 (1990).
[9] C. Mayol, R. Toral, and C. R. Mirasso, Phys. Rev. A **59**, 4690 (1999).
[10] J. Guckenheimer and P. Holmes, *Nonlinear Oscillations, Dynamical Systems and Bifurcation of Vector Fields* (Springer-Verlag, Berlin, 1983).
[11] M. San Miguel, R. Montagne, A. Amengual, and E. Hernández-García, in *Instabilities and Nonequilibrium Structures V*, edited by E. Tirapegui and W. Zeller (Kluwer Academic, Dordrecht, 1996).
[12] R. Montagne, E. Hernández-García, and M. San Miguel, Physica D **96**, 47 (1996).
[13] H. Haken, *Laser Theory* (Springer-Verlag, New York, 1984).
[14] W. A. van der Graaf, Ph.D. thesis, Vrije Universiteit, Amsterdam, 1997.
[15] G. P. Agrawal and N. K. Dutta, *Long-Wavelength Semiconductor Lasers* (Van Nostrand, Reinhold, New York, 1986).
[16] M. Sargent, M. O. Scully, and W. E. Lamb, Jr., *Laser Physics* (Addison-Wesley, Reading, MA, 1974).

[17] H. Risken, *The Fokker-Plank Equation* (Springer-Verlag, Berlin, 1989).
[18] M. Zimmermann, M. Natiello, and H. G. Solari, Chaos **11**, 500 (2001).
[19] R. Adler, Proc. IRE **34**, 351 (1946), reprinted in Proc. IEEE **61**, 1380 (1973).
[20] S. H. Strogatz, *Nonlinear Dynamics and Chaos* (Addison-Wesley, Reading, 1994).
[21] Y. Kuznetsov, *Elements of Applied Bifurcation Theory*, Applied Mathematical Sciences Vol. 112 (Springer, New York, 1995).
[22] E. Doedel, F. Fairgrieve, B. Sandstebe, A. Champeneys, Yu. Kuznetzov, and S. Wang, *AUTO97: Continuation and bifurcation software for ordinary differential equations*, http://indy.cs.concordia.ca/auto/main.html.
[23] S. Schecter, SIAM (Soc. Ind. Appl. Math.) J. Math. Anal. **18**, 1142 (1987).
[24] C. Mayol, M. A. Natiello, and M. G. Zimmermann, Int. J. Bifurcation Chaos Appl. Sci. Eng. **11**, 2587 (2001).
[25] A. Khibnik, B. Krauskopf, and C. Rousseau, Nonlinearity **11**, 1505 (1998).
[26] B. Krauskopf, Exp. Math. **3**, 107 (1994).
[27] S. Wieczorek, B. Krauskopf, and D. Lenstra, Proc. SPIE **3944**, 602 (2000).
[28] B. Krauskopf, S. Wieczorek, and D. Lenstra, Proc. SPIE **3944**, 612 (2000).
[29] B. Krauskopf, S. Wieczorek, and D. Lenstra, Appl. Phys. Lett. **77**, 1611 (2000).
[30] S. Wieczorek, B. Krauskopf, and D. Lenstra, Opt. Lett. **26**, 816 (2001).
[31] S. Wieczorek, B. Krauskopf, and D. Lenstra, Phys. Rev. E **64**, 056201 (2001).
[32] M. Zimmermann, M. Natiello, and H. Solari, Physica D **109**, 293 (1997).
[33] B. Krauskopf and W. Wieczorek, University of Bristol, Report No. 2001.21 (unpublished).
[34] H. Haken, *Synergetics* (Springer-Verlag, Berlin, 1983).
[35] M. San Miguel and R. Toral, in *Instabilities and Nonequilibrium Structures VI*, edited by E. Tirapegui and W. Zeller (Kluwer Academic, Dordrecht, 1997).
[36] R. Graham, in *Instabilities and Nonequilibrium Structures*, edited by E. Tirapegui and D. Villaroel (Reidel, Dordrecht, 1987); in *Instabilities and Nonequilibrium Structures III*, edited by E. Tirapegui and W. Zeller (Reidel, Dordrecht, 1991).